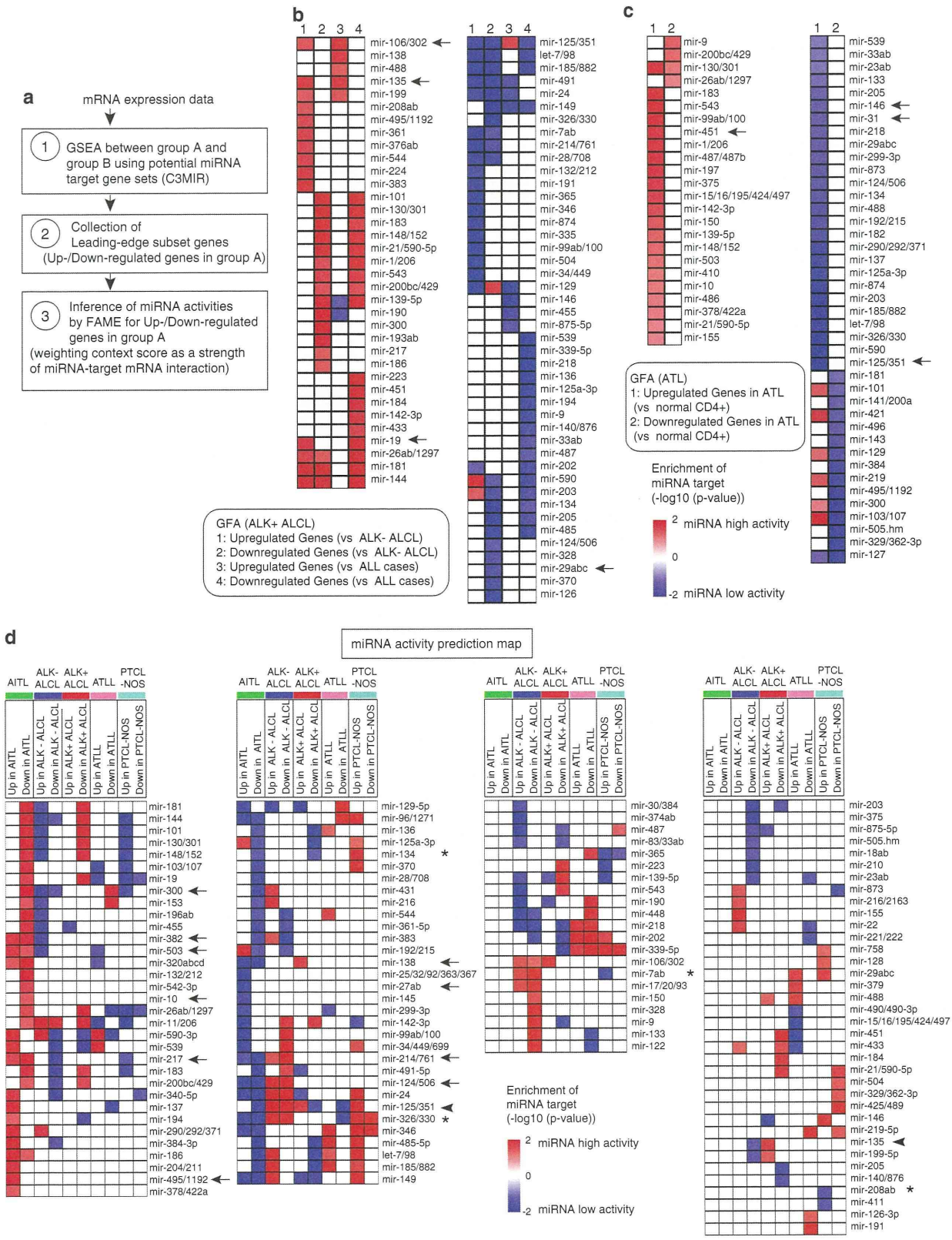

Figure 1. Prediction of miRNA activities in peripheral T cell lymphoma by GFA. (**a**) Outline of GFA. The details of GFA have been described in Supplementary Information. (**b**) GFA in ALK+ ALCL. GFA was performed between ALK+ and ALK− ALCL, and between ALK+ ALCL and all cases of PTCL in the gene expression profile of T cell lymphoma (GSE19069). miRNAs with $P > 0.05$ are shown as white squares. miRNAs indicated by arrows have been discussed in the main text. (**c**) GFA in ATL. GFA was performed between ATL cells and CD4-positive normal T cells in the gene expression profile of ATL (GSE33615). miRNAs with $P > 0.1$ are shown as white squares. miRNAs indicated by arrows have been discussed in the main text. (**d**) GFA in PTCL subtypes. For four major T cell lymphoma subtypes (AITL, ALK+ ALCL, ATLL and PTCL-NOS), GFA was performed between each lymphoma subtype and all cases of PTCL in GSE19069 data set. miRNAs with $P > 0.05$ are shown as white squares. miRNAs indicated by arrows (for AITL), arrowheads (for ALK+ ALCL and ATLL) and asterisks (for PTCL-NOS) have been discussed in the main text.

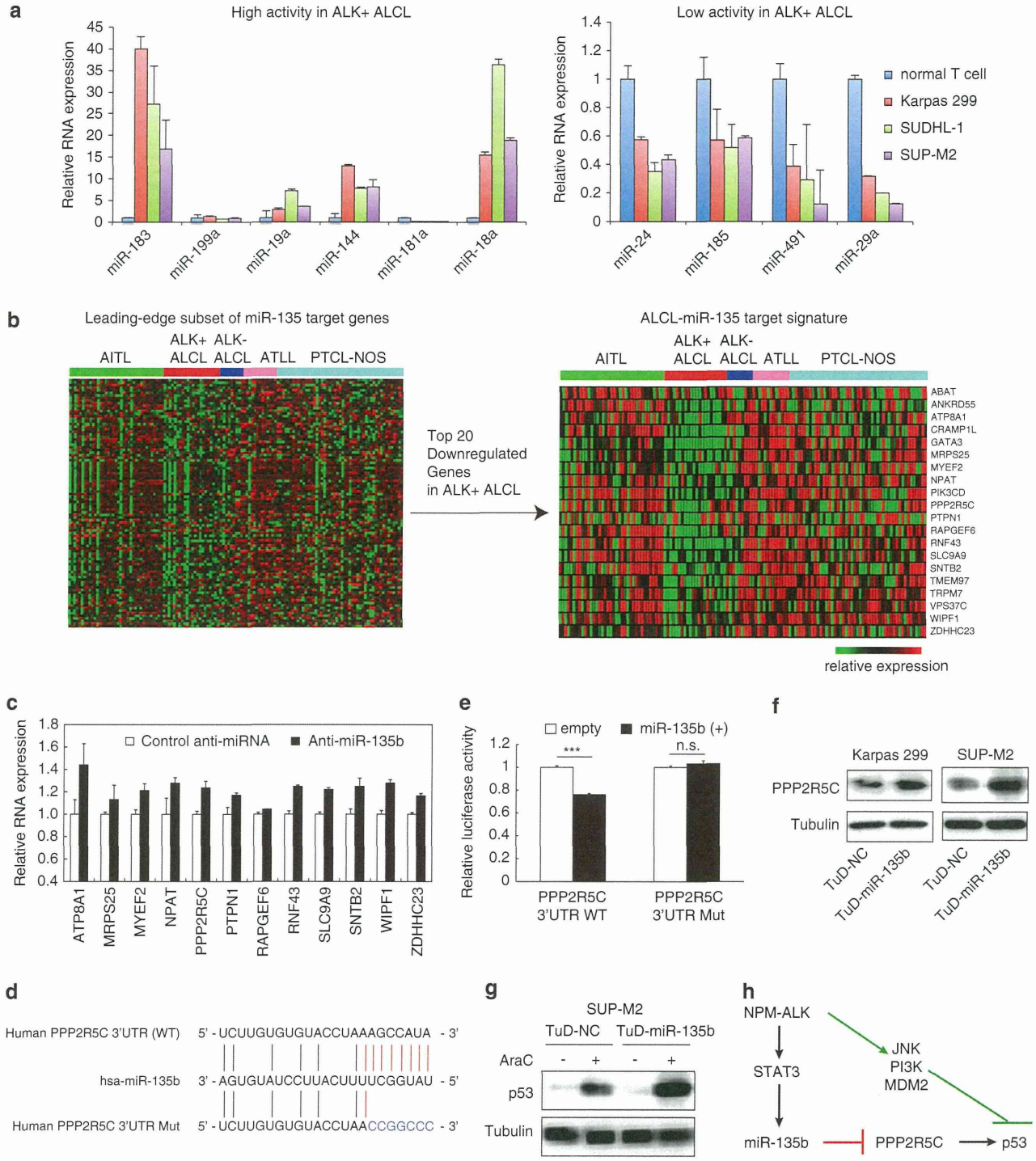

Figure 2. Validation of GFA results and identification of miR-135b–PPP2R5C–p53 axis in ALK+ ALCL. (**a**) Expression of mature miR-183, -199a, -19a, -144, -181a, -18a, -24, -185, -491 and -29a in normal T lymphocytes and NPM–ALK+ ALCL cell lines (Karpas 299, SUDHL-1 and SUP-M2), detected by qRT-PCR analysis. (**b**) ALCL–miR-135 target signature. Among the leading-edge gene set of miR-135 target genes (left) in GFA, the top 20 downregulated genes in ALK+ ALCL compared with other lymphoma subtypes were extracted as highly potential miR-135b target genes (ALCL–miR-135 target signature) in ALK+ ALCL (right). (**c**) Effects of miR-135b inhibition on mRNA expression levels of ALCL–miR-135 target genes in Karpas 299 cells. After transfection with miRNA inhibitors, Karpas 299 cells were subjected to qRT-PCR analysis. (**d**) Sequence alignment between miR-135b and its putative binding sites in PPP2R5C 3′-untranslated region (UTR). (**e**) miR-135b targets PPP2R5C. Luciferase activity of the PPP2R5C 3′-UTR reporter constructs with the wild-type or mutated target site (shown in (**d**)) in HEK293T cells co-transfected with an empty vector or pri-miR-135b expression vector (miR-135b (+)). $^{***}P<0.001$; n.s., not significant. (**f**) Elevated expression of PPP2R5C protein by miR-135b inhibition in ALCL cells. Karpas 299 and SUP-M2 cells were infected with lentivirus harboring TuD-NC or TuD–miR-135b, and applied to immunoblot analysis. (**g**) Enhancement of DNA damage-mediated p53 induction by miR-135b suppression in SUP-M2 cells. SUP-M2 cells were infected with lentivirus harboring TuD-NC or TuD–miR-135b, treated by AraC (1 μM, 24 h), and applied to immunoblot analysis. (**h**) Suppression of the p53 pathway by NPM–ALK–miR-135b–PPP2R5C axis. Green lines indicate alternative cascades connecting NPM–ALK to the inhibition of p53 activities shown in other study.[14]

downregulation in ALK+ ALCL, respectively.[7,8] We used the results of comprehensive gene expression profiling on 144 PTCL patients, including AITL, ALK+ ALCL, ALK− ALCL, adult T cell leukemia/lymphoma (ATLL) and PTCL not-otherwise-specified (PTCL-NOS).[9] We performed GFA between ALK+ ALCL and ALK− ALCL, and between ALK+ ALCL and all PTCL cases so that GFA could be applied for more than two groups. GFA results successfully predicted high activity of miR-106 and miR-135 and low activity of miR-29 in ALK+ ALCL both in comparison with ALK− ALCL and with all cases (Figure 1b). In miR-17–92 cluster, miR-19 was predicted to be active.

Recently published miRNA and mRNA profiling in the primary clinical samples of adult T cell leukemia (ATL) highlighted the loss of miR-31 in ATL.[10] GFA applied to this data set consistently showed low miR-31 activity in ATL (Figure 1c). GFA results also highlighted altered activities of several miRNAs such as miR-125 (low), miR-146 (low) and miR-451 (high), which matched the results of miRNA expression profiling in this data set.

As summarized in Figure 1d, GFA for five PTCL subtypes showed the characteristic patterns of different miRNA activities in distinct lymphoma subtypes. For example, miR-10, -217, -300, -382, -495 and -503 were predicted to be active in AITL (Figure 1d, Arrows). Conversely, miR-27, -124, -138 and -214 were predicted to be underactive in AITL (Figure 1d, Arrows). GFA showed high activity of miR-135 specifically in ALK+ ALCL, and low activity of miR-125 in ATLL (Figure 1d, Arrowhead). The different results for ATLL in Figures 1c and d may be due to the heterogeneity in the clinical entities of ATLL, differences in comparison targets (normal CD4 T cells and other subtypes) and low tumor content in clinical samples.

In PTCL-NOS, several miRNAs such as miR-326 and -134 were predicted to be active, and other miRNAs including miR-7 and -208 were predicted to be underactive (Figure 1d, Asterisks). It has been recently shown that the most upregulated (miR-326, -663b and -711) and downregulated (miR-203 and -205) miRNAs in cutaneous T cell lymphoma distinguish cutaneous T cell lymphoma and PTCL-NOS from benign skin diseases.[11] Among these miRNAs, GFA predicted high activity of miR-326 with a $P<0.05$ threshold, and low activity of miR-205 with a $P<0.1$ threshold. This implies that these miRNAs may also be useful for the classification of PTCL-NOS and other lymphoma subtypes, in addition to the separation of PTCL-NOS from benign diseases. These results indicate a good correlation between the alteration in miRNA expression levels directly measured in the literature and changes in miRNA activities inferred from independent published gene expression profiling, suggesting that GFA can predict biologically relevant changes in miRNA activities from mRNA profiling. As global miRNA profiling has not been reported in PTCL, this prediction should be assessed further in future investigations. Differences in tumor content in clinical samples, especially low content in AITL and PTCL-NOS, should be also considered for interpretation.

We next investigated whether mRNA profiling can be utilized for reverse identification of disease-related miRNAs and target identification of disease-related miRNAs. We investigated the expression levels of GFA-supported miRNAs in ALK+ ALCL. As shown in Figure 2a, high expression of miR-183, -18a and -19a was confirmed in three ALCL cell lines harboring *NPM–ALK* fusion; Karpas 299, SUDHL-1 and SUP-M2 cells, relative to normal T cells. In addition to miR-29a, downregulation of miR-24, -185 and -491 was also observed. Furthermore, upregulation of miR-183, -18a and -19a was confirmed in human primary ALK+ ALCL samples, relative to reactive lymph node and ALK− ALCL samples (Supplementary Figure S1). Interestingly, we observed no significant changes in miR-199a and miR-181a in the cell lines, but these miRNAs were upregulated in clinical samples (Figure 2a and Supplementary Figure S1). Considering that GFA is based on the expression profiling of clinical samples, the upregulation of miR-199a and miR-181a may be attributable to the *in vivo* reaction in ALCL.

GFA generates a list of probable target genes for each miRNA for further convenient experimental validation of miRNA–mRNA interactions. Consistent with our report,[8] GFA revealed that high miR-135b activity seems to leave its footprint on clinical ALCL transcriptome. Among the leading-edge gene subset of potential miR-135 target genes that were downregulated in ALK+ ALCL, the top 20 downregulated genes (referred to as 'ALCL–miR-135 target signature') included several genes such as *GATA3*, *PPP2R5C* and *RAPGEF6* (Figure 2b). Our previous report showed that GATA3 is a direct target of miR-135b in ALCL. We observed that a large proportion of the 'ALCL–miR-135 target signature' (ATP8A1, MRPS25, MYEF2, NPAT, PPP2R5C, PTPN1, RAPGEF6, RNF43, SLC9A9, SNTB2, WIPF1 and ZDHHC23) was indeed upregulated by miR-135b inhibition in Karpas 299 ALCL cells (Figure 2c), suggesting the direct contribution of miR-135b to the downregulation of the 'ALCL–miR-135 target signature' in ALCL. We defined a deregulation index for target gene sets by averaging normalized gene expression values and investigated the association between the 'ALCL–miR-135 target signature', which potentially reflects miR-135b activity, and interleukin-17-producing immunophenotype rendered by miR-135b overexpression in ALCL.[8] The deregulation index values of the 'ALCL–miR-135 target signature' and Th17-related genes were clearly low and high in ALK+ ALCL, respectively (Supplementary Figure S2a), and these two values showed a negative correlation (Supplementary Figure S2b). Comparable results were confirmed in another data set for T cell lymphoma (Supplementary Figure S2c).[12] Similar approach also suggested the potential interaction between miR-125 with low activity in ATLL and several known targets, including IRF4, IKZF4, KLF13, ETS1, ARID3B and MCL1 (Supplementary Figure S3).

Although molecular functions are largely unknown in most 'ALCL–miR-135 target signature' genes, we focused on PPP2R5C, which encodes protein phosphatase 2A (PP2A) regulatory subunit B56γ, as PP2A B56γ mediates the DNA-damage-induced dephosphorylation and stabilization of p53, and thus exerts a tumor-suppressor function.[13] Exogenous miR-135b suppressed the translational efficiency of PPP2R5C 3′-untranslated region depending on the target site (Figures 2d and e). Knockdown of miR-135b by TuD RNA increased the protein expression levels of PPP2R5C in ALCL cells (Figure 2f), indicating PPP2R5C as an endogenous miR-135b target. Consistent with the positive effect of PPP2R5C on p53, miR-135b inhibition enhanced p53 accumulation by the DNA damaging agent AraC in p53-wild-type SUP-M2 cells (Figure 2g). Therefore, NPM–ALK may suppress p53 activity through miR-135b–PPP2R5C axis, and upregulation of MDM2 and JNK activities reported previously[14] (Figure 2h).

Our findings reinforce the possibility of inference of miRNA regulation underlying the mRNA profiles from numerous gene expression data sets in publicly accessible repositories, even if these studies included one-sided mRNA profiles and did not design miRNA profiling. The results in Figures 2b and c; and Supplementary Figure S2 suggest that a subset of miRNA target genes can represent the biological activity of corresponding miRNAs. Png *et al.*[15] recently showed similar approach, in which eight miR-126 target genes reflect the metastasis-suppressor activity of miR-126 and strongly correlate with metastatic relapse in human breast cancer. GFA may be useful for the identification of such representative miRNA target genes. The present study suggests that combinational investigation of gene expression profiling and computational miRNA activity predictions may yield a wide platform for assessment of miRNA involvement in various disease processes, together with miRNA profiling.

CONFLICT OF INTEREST

The authors declare no conflict of interest.

ACKNOWLEDGEMENTS

We thank Nishimori H, Morishita Y and Mihira H for their discussion and skilled technical assistance; and all the members of the Department of Molecular Pathology, the University of Tokyo. This work was supported by KAKENHI (Grants-in-Aid for Young Scientists (A) (no. 24689018) and for Scientific Research on Innovative Areas 'RNA regulation' (no. 23112702), and 'Integrative research on cancer microenvironment network' (no. 22112002)), the Global Center of Excellence Program for 'Integrative Life Science Based on the Study of Biosignaling Mechanisms' from the Ministry of Education, Culture, Sports, Science, and Technology of Japan, and the Cell Science Research Foundation.

AUTHOR CONTRIBUTIONS

HIS designed the research, performed experiments and analyses, and wrote the paper; HM provided the key materials, and performed the experiments and analyses; MN, TY, NK and KS provided clinical samples; and KS and KM supervised the project and wrote the paper.

HI Suzuki[1], H Matsuyama[1], M Noguchi[2], T Yao[3], N Komatsu[4], H Mano[5,6], K Sugimoto[4,7] and K Miyazono[1]
[1]Department of Molecular Pathology, Graduate School of Medicine, The University of Tokyo, Bunkyo-ku, Japan;
[2]Department of Hematology, Juntendo Urayasu Hospital, Urayasu-shi, Japan;
[3]Department of Human Pathology, Juntendo University Graduate School of Medicine, Bunkyo-ku, Japan;
[4]Division of Hematology, Department of Internal Medicine, Juntendo University Graduate School of Medicine, Bunkyo-ku, Japan;
[5]Department of Medical Genomics, Graduate School of Medicine, The University of Tokyo, Bunkyo-ku, Japan;
[6]Division of Functional Genomics, Jichi Medical University, Shimotsuke-shi, Japan and
[7]Department of Hematology and Oncology, JR Tokyo General Hospital, Shibuya-ku, Japan
E-mail: hisuzuki-tky@umin.ac.jp
or miyazono@m.u-tokyo.ac.jp

REFERENCES

1 Schotte D, Pieters R, Den Boer ML. MicroRNAs in acute leukemia: from biological players to clinical contributors. *Leukemia* 2012; **26**: 1–12.
2 Akbari Moqadam F, Pieters R, den Boer ML. The hunting of targets: challenge in miRNA research. *Leukemia* 2013; **27**: 16–23.
3 Pritchard CC, Cheng HH, Tewari M. MicroRNA profiling: approaches and considerations. *Nat Rev Genet* 2012; **13**: 358–369.
4 Callari M, Dugo M, Musella V, Marchesi E, Chiorino G, Grand MM *et al.* Comparison of microarray platforms for measuring differential microRNA expression in paired normal/cancer colon tissues. *PLoS One* 2012; **7**: e45105.
5 Suzuki HI, Mihira H, Watabe T, Sugimoto K, Miyazono K. Widespread inference of weighted microRNA-mediated gene regulation in cancer transcriptome analysis. *Nucleic Acids Res* 2013; **41**: e62.
6 Merkel O, Hamacher F, Laimer D, Sifft E, Trajanoski Z, Scheideler M *et al.* Identification of differential and functionally active miRNAs in both anaplastic lymphoma kinase (ALK)+ and ALK- anaplastic large-cell lymphoma. *Proc Natl Acad Sci USA* 2010; **107**: 16228–16233.
7 Desjobert C, Renalier MH, Bergalet J, Dejean E, Joseph N, Kruczynski A *et al.* MiR-29a down-regulation in ALK-positive anaplastic large cell lymphomas contributes to apoptosis blockade through MCL-1 overexpression. *Blood* 2011; **117**: 6627–6637.
8 Matsuyama H, Suzuki HI, Nishimori H, Noguchi M, Yao T, Komatsu N *et al.* miR-135b mediates NPM-ALK-driven oncogenicity and renders IL-17-producing immunophenotype to anaplastic large cell lymphoma. *Blood* 2011; **118**: 6881–6892.
9 Iqbal J, Weisenburger DD, Greiner TC, Vose JM, McKeithan T, Kucuk C *et al.* Molecular signatures to improve diagnosis in peripheral T-cell lymphoma and prognostication in angioimmunoblastic T-cell lymphoma. *Blood* 2010; **115**: 1026–1036.
10 Yamagishi M, Nakano K, Miyake A, Yamochi T, Kagami Y, Tsutsumi A *et al.* Polycomb-mediated loss of miR-31 activates NIK-dependent NF-kappaB pathway in adult T cell leukemia and other cancers. *Cancer Cell* 2012; **21**: 121–135.
11 Ralfkiaer U, Hagedorn PH, Bangsgaard N, Lovendorf MB, Ahler CB, Svensson L *et al.* Diagnostic microRNA profiling in cutaneous T-cell lymphoma (CTCL). *Blood* 2011; **118**: 5891–5900.
12 Piccaluga PP, Agostinelli C, Califano A, Rossi M, Basso K, Zupo S *et al.* Gene expression analysis of peripheral T cell lymphoma, unspecified, reveals distinct profiles and new potential therapeutic targets. *J Clin Invest* 2007; **117**: 823–834.
13 Li HH, Cai X, Shouse GP, Piluso LG, Liu X. A specific PP2A regulatory subunit, B56gamma, mediates DNA damage-induced dephosphorylation of p53 at Thr55. *EMBO J* 2007; **26**: 402–411.
14 Cui YX, Kerby A, McDuff FK, Ye H, Turner SD. NPM-ALK inhibits the p53 tumor suppressor pathway in an MDM2 and JNK-dependent manner. *Blood* 2009; **113**: 5217–5227.
15 Png KJ, Halberg N, Yoshida M, Tavazoie SF. A microRNA regulon that mediates endothelial recruitment and metastasis by cancer cells. *Nature* 2012; **481**: 190–194.

Supplementary Information accompanies this paper on the Leukemia website (http://www.nature.com/leu)

STK10 missense mutations associated with anti-apoptotic function

KAZUTAKA FUKUMURA[1,2], YOSHIHIRO YAMASHITA[4], MASAHITO KAWAZU[1], EIRIN SAI[1], SHIN-ICHIRO FUJIWARA[5], NAOYA NAKAMURA[6], KENGO TAKEUCHI[7], MIZUO ANDO[1], KOHEI MIYAZONO[2], TOSHIHIDE UENO[4], KEIYA OZAWA[5] and HIROYUKI MANO[1,3,4,8]

Departments of [1]Medical Genomics, [2]Molecular Pathology and [3]Cellular Signaling, Graduate School of Medicine, The University of Tokyo, Tokyo 113-0033; [4]Division of Functional Genomics and [5]Department of Hematology, Jichi Medical University, Tochigi 329-0498; [6]Department of Pathology, Tokai University School of Medicine, Kanagawa 259-1193; [7]Pathology Project for Molecular Targets, The Cancer Institute of the Japanese Foundation for Cancer Research, Tokyo 135-8550; [8]CREST, Japan Science and Technology Agency, Saitama 332-0012, Japan

Received May 8, 2013; Accepted June 12, 2013

DOI: 10.3892/or.2013.2605

Abstract. Peripheral T-cell lymphoma (PTCL) is an aggressive lymphoma with a 5-year overall survival rate of <30%. To identify carcinogenesis-related genes in PTCL, we conducted high-throughput resequencing of target-captured cDNA in a PTCL specimen, revealing a total of 19 missense mutations among 18 independent genes. One of such substitutions, c.2201G>A in *STK10* cDNA, replaces an arginine residue to a histidine (R634H) in the encoded protein. Of note, while wild-type STK10 suppresses NF-κB activity and potentiates dexamethasone-induced apoptosis, the R634H change significantly decreases such pro-apoptotic activity. This c.2201G>A change of *STK10* was also identified in another PTCL specimen, but now registered as a single nucleotide polymorphism in the latest dbSNP database. Furthermore, other somatic mutations of STK10 have been reported, and we now reveal that some of them (L85P and K277E) have more profound anti-apoptotic effects compared to R634H. These results suggest that *STK10* functions as a tumor suppressor gene, and that dysfunction of STK10 activity either through polymorphism or somatic mutations may confer anti-apoptotic effects contributing to carcinogenesis.

Introduction

Various genetic alterations such as point mutations, insertions/deletions (indels) and gene fusions directly participate in human carcinogenesis. Some of such changes confer growth advantage to cancer cells, and targeting their encoded proteins is one of the most effective means to treat cancer. Activating mutations in *EGFR* (1) or the gene fusion between *EML4* and *ALK* (2) are, for instance, identified in subsets of non-small cell lung cancer (NSCLC), and reagents targeting EGFR or ALK are proved clinically effective against NSCLC positive for the corresponding genetic lesions (3,4).

Peripheral T-cell lymphoma (PTCL) is a subdivision of non-Hodgkin's malignant lymphoma (5). In contrast to the improved prognosis for individuals with B-cell lymphoma with recent treatment modalities, most subtypes of PTCL still have a 5-year survival rate of only <30% (6). Molecular mechanism for PTCL carcinogenesis is mainly enigmatic, except for the facts that i) a part of PTCL is associated with infection with Epstein-Barr virus (EBV) or human T-lymphotropic virus type I (HTLV-I), and ii) activating ALK fusions are found in the anaplastic large cell lymphoma (ALCL) subtype. Given the fact that an ALK inhibitor is effective in the treatment of ALCL (7), identification of essential growth drivers in other subsets of PTCL is urgently needed.

While exome sequencing of cancer specimens is used for the detection of somatic mutations in the cancer genome, such approach fails to detect gene fusions, because gene fusions usually take place at intronic regions. To simultaneously detect point mutations/indels/gene fusions in a single experiment, we previously reported the 'cDNA capture system' that conducts massive resequencing on purified cDNAs for cancer-related genes (8). Herein we applied such technology to the cDNAs isolated from a PTCL specimen, and discovered a STK10 amino acid substitution that turned out to exert anti-apoptotic effects. While this amino acid change was recently deposited as a single nucleotide polymorphism (SNP) in the 1000 genome database (http://www.1000genomes.org), we also confirmed that other nonsynonymous, somatic mutations within *STK10* confer marked anti-apoptotic activity. These results suggest that STK10 may contribute to carcinogenesis, either through polymorphism or somatic mutations, by suppressing apoptotic signaling in cancer.

Materials and methods

Cell lines and specimens. PTCL specimens were collected in Fukushima Medical University and The Cancer Institute.

Correspondence to: Professor Hiroyuki Mano, Department of Cellular Signaling, Graduate School of Medicine, University of Tokyo, 7-3-1 Hongo, Bunkyo-ku, Tokyo 113-0033, Japan
E-mail: hmano@m.u-tokyo.ac.jp

Key words: tumor suppressor gene, apoptosis, NF-κB

A human embryonic kidney 293T (HEK293) cell line was obtained from American Type Culture Collection (ATCC: Manassas, VA, USA), and maintained in Dulbecco's modified Eagle's medium-F12 medium (Invitrogen, Carlsbad, CA, USA) supplemented with 10% fetal bovine serum (FBS) and 2 mM L-glutamine (both from Invitrogen). An IL-2-dependent mouse cytotoxic T-cell line, CTLL-2, and a human T-cell line, Jurkat, were both obtained from ATCC, and maintained in RPMI1640 medium (Invitrogen) supplemented with 10% FBS. Mouse recombinant IL-2 (Peprotech, Rocky Hill, NJ, USA) was added to the culture medium of CTLL-2 at the concentration of 2 ng/ml. Total RNA was extracted from cell lines and a PTCL specimen with an RNeasy mini kit (Qiagen, Valencia, CA, USA), and was subjected to reverse transcriptase (RT) with an oligo-dT primer. Written informed consent was obtained from the subjects who provided cancer specimens, and the study was approved by the human ethics committee of the University of Tokyo, Jichi Medical University, Fukushima Medical University, and The Cancer Institute of the Japanese Foundation for Cancer Research.

Resequencing of target-captured cDNA in a PTCL specimen. Resequencing with a custom cDNA-capture system was performed as previously described (8). In brief, RNA probes of 120 bases were designed to interrogate cDNAs of 906 human protein-coding genes, and were synthesized by Agilent Technologies (Santa Clara, CA, USA). Hybridization of cDNA fragments isolated from a PTCL specimen to the RNA probes was performed according to the protocols recommended for the SureSelect Target Enrichment system (Agilent Technologies). Purified cDNA fragments were then subjected to deep sequencing with a Genome Analyzer IIx (GAIIx; Illumina, San Diego, CA, USA) for 76 bases from both ends by the paired-end sequencing system.

Plasmid construction. The full-length cDNA for the wild-type or the R634H mutant of STK10 was amplified by PCR from cDNA of a PTCL specimen. The cDNAs for other mutant forms of STK10 were further generated by a polymerase chain reaction (PCR)-based mutagenesis approach. The cDNA for PLK1, IKK-α, IKK-β or IKK-γ was amplified by PCR from our cancer cell lines.

Luciferase-based reporter assay. HEK293 cells were transfected with the expression plasmids, a promoter-less *Renilla* luciferase plasmid pGL-4.70 (Promega, Madison, WI, USA), and firefly luciferase-based reporter plasmid for Fos (pFL700) (9), Myc (pHXL) (10), NF-κB (Stratagene, La Jolla, CA, USA), Bcl-xL (11), Notch (pGa981-6) (12), Wnt (TOP-flash, Upstate Biotechnology, Lake Placid, NY, USA) or Rho (pSRE.L) (13) signaling pathway. Luciferase activities were determined with the Dual-Luciferase Reporter Assay System (Promega), and the firefly luciferase activities were normalized to the *Renilla* luciferase activities.

Quantitative real-time RT-PCR. Quantitative real-time RT-PCR was performed with QuantiTect SYBR Green PCR kit (Qiagen) and an Applied Biosystems 7900HT Fast Real-Time PCR System. The PCR conditions include the first incubation at 50°C for 2 min and then 95°C for 15 min, followed by 60 cycles of 94°C for 15 sec and 60°C for 30 sec and 72°C for 1 min. Relative expression levels of target mRNAs to *GAPDH* were normalized to those in the mock-transfected cells. The primer sequences used for the PCR reactions were: 5'-TTCATTCCTGGCAAGTGGATCATT-3' and 5'-ATGG CAGCATCATTGTTCTCATCA-3' for *TLR2*, 5'-TGACAAC CTTCTGGTTGGTAGGGA-3' and 5'-CCAAGGTCATGGT TGTCCAAAGAC-3' for *BCL2*, 5'-AAGAATCACCAGCA GCAAGTGTCC-3' and 5'-TTGGGTTGTGGAGTGAGTG TTCAA-3' for *CCL2*, and 5'-CCAGGTGGTCTCCTCTGAC TTCAA-3' and 5'-CACCCTGTTGCTGTAGCCAAATTC-3' for *GAPDH*.

Antibodies, immunoprecipitation and immunoblotting. Antibodies used in this study were: anti-FLAG M2 (Sigma-Aldrich, St. Louis, MO, USA), anti-PLK1 (Santa Cruz Biotechnology, Santa Cruz, CA, USA), anti-phospho-PLK1 (BD Pharmingen, San Jose, CA, USA), anti-ACTB (Cell Signaling Technology, Danvers, MA, USA), anti-mouse IgG and anti-rabbit IgG (both from GE Healthcare, Piscataway, NJ, USA). HEK293 cells were transfected with the appropriate expression vectors, and then lysed in lysis buffer [1% NP-40, 50 mM Tris-HCl (pH 7.4), 150 mM NaCl, 1 mM NaF, 1 mM Na_3VO_4, 1 mM phenylmethylsulfonyl fluoride and aprotinin]. Target proteins were purified by incubation of the cell lysates with appropriate antibodies and Protein G Sepharose Fast Flow (Sigma-Aldrich) for 3 h at 4°C. Immunoblot analyses were visualized with SuperSignal West Femto Maximum Sensitivity Substrate (Thermo Scientific, Waltham, MA, USA).

In vitro kinase assay. Immunoprecipitates were washed with kinase buffer [50 mM NaCl, 50 mM Tris-HCl (pH 7.4), 10 mM $MgCl_2$, 10 mM $MnCl_2$ and 0.1 mM Na_3VO_4], and then incubated in kinase buffer containing [γ-^{32}P]ATP (Perkin-Elmer, Boston, MA, USA) and histone H2A protein (New England BioLabs, Ipswich, MA, USA) for 30 min at room temperature.

Dexamethasone-induced apoptosis assay. CTLL-2 cells were infected with retrovirus expressing *STK10* and the blasticidin-resistant gene, and cultured under the presence of 10 μg/ml blasticidin (InvivoGen, San Diego, CA, USA). Blasticidin-resistant cells were then treated with 1 μM dexamethasone (Sigma-Aldrich), and cell number was determined every 24 h with CellTiter-Glo Luminescent Cell Viability Assay (Promega). At 72 h after treatment with dexamethasone, CTLL-2 cells were collected and subjected to apoptosis assay with flow cytometry (FACSCanto II; BD Biosciences, San Jose, CA, USA) using Annexin V/propidium iodide (PI) staining kit (eBioscience, San Diego, CA, USA).

Results

Identification of STK10(R634H) in a PTCL specimen. To identify transforming genes in PTCL, cDNAs for cancer-related genes (n=906) (8) were isolated from a PTCL specimen obtained from a 25 year-old male negative for EBV and HTLV-I infection, and subjected to deep sequencing with GAIIx. We thus obtained a total of 69,552,278 independent, high-quality reads that mapped to 868 cDNAs (95.8%).

Table I. Nonsynonymous mutations detected in a PTCL specimen.

Gene symbol	GenBank accession no.	Nucleotide change	Read coverage	Mismatch reads (%)	Amino acid change
AXL[a]	NM_001699	c.1506G>T	x156	59.0	W439L
CDC7	NM_003503	c.1732C>G	x317	47.0	H523D
CDC7	NM_003503	c.1751A>G	x298	48.3	N529S
CREBBP	NM_001079846	c.2478G>T	x470	54.7	Q758H
E2F1	NM_005225	c.1399G>A	x126	30.2	G420D
EIF2AK4	NM_001013703	c.3268G>A	x239	46.0	R1073H
FERMT3	NM_031471	c.2080G>T	x48	56.3	R644L
FOXO3[a]	NM_201559	c.2013G>C	x1001	41.3	G566A
LRRK2[a]	NM_198578	c.4314G>A	x166	43.4	R1398H
MAPK7[a]	NM_139033	c.2475G>A	x287	61.7	G697R
PDGFRB[a]	NM_002609	c.3441G>A	x129	35.7	R991H
PTCH1	NM_000264	c.4423C>T	x60	63.3	P1412L
PTCH2[a]	NM_003738	c.2975C>T	x502	61.6	T988M
RPS6KA2[a]	NM_021135	c.1202G>A	x293	41.0	R328Q
RPS6KB2[a]	NM_003952	c.882C>T	x446	54.0	P267L
SOS2	NM_006939	c.668A>T	x338	49.1	E190D
STK4	NM_006282	c.962G>A	x7195	49.1	R291Q
STK10[a]	NM_005990	c.2201G>A	x462	58.7	R634H
TRIM33	NM_015906	c.1049C>T	x599	44.9	A322V

[a]Registered in the 1000 genome project database.

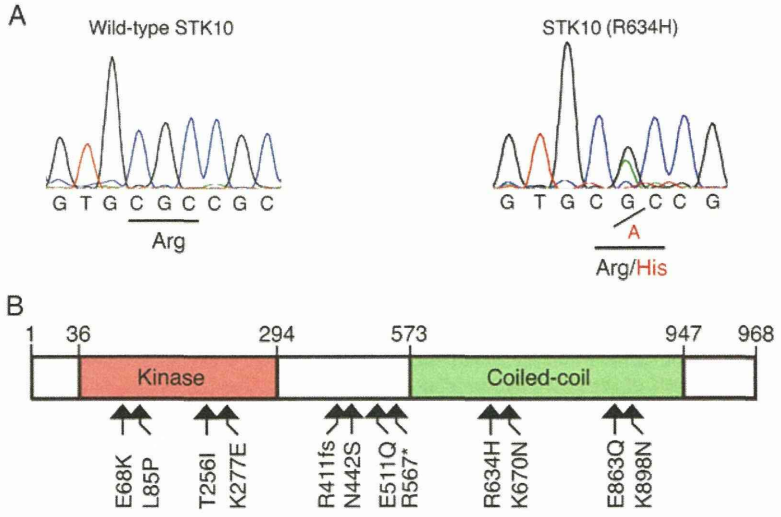

Figure 1. Identification of STK10(R634H) in a PTCL specimen. (A) Genomic DNA corresponding to the R634 position of STK10 protein was amplified by PCR from a PTCL specimen, and subjected to Sanger sequencing. Nucleotide and amino acid substitutions are shown red. (B) Schematic representation of STK10 protein structure with amino acid number shown at the top. The positions of amino acid changes reported in this study are depicted at the bottom.

Screening of missense mutations, insertions, deletions and fusion genes through our in-house computational pipeline (8) revealed a total of 19 nonsynonymous mutations but no indels or gene fusions, which were further confirmed by Sanger sequencing (Table I). It should be noted, however, that 9 of the 19 nonsynonymous mutations were recently registered as single nucleotide polymorphisms (SNPs) in the 1000 genome project (http://www.1000genomes.org) after our initial analysis.

One of the 19 nonsynonymous mutations was a nucleotide substitution of G-to-A at position 2201 of human *STK10* cDNA (GenBank accession number, NM_005990) that was later deposited as an SNP (rs115974403). Sequencing of this position in genomic DNA of the same specimen further confirmed this substitution, which results in replacement of an arginine residue at amino acid position 634 with a histidine residue (R634H) (Fig. 1A). We also searched STK10 mutations among our human cancer specimens (n=76), cancer cell lines

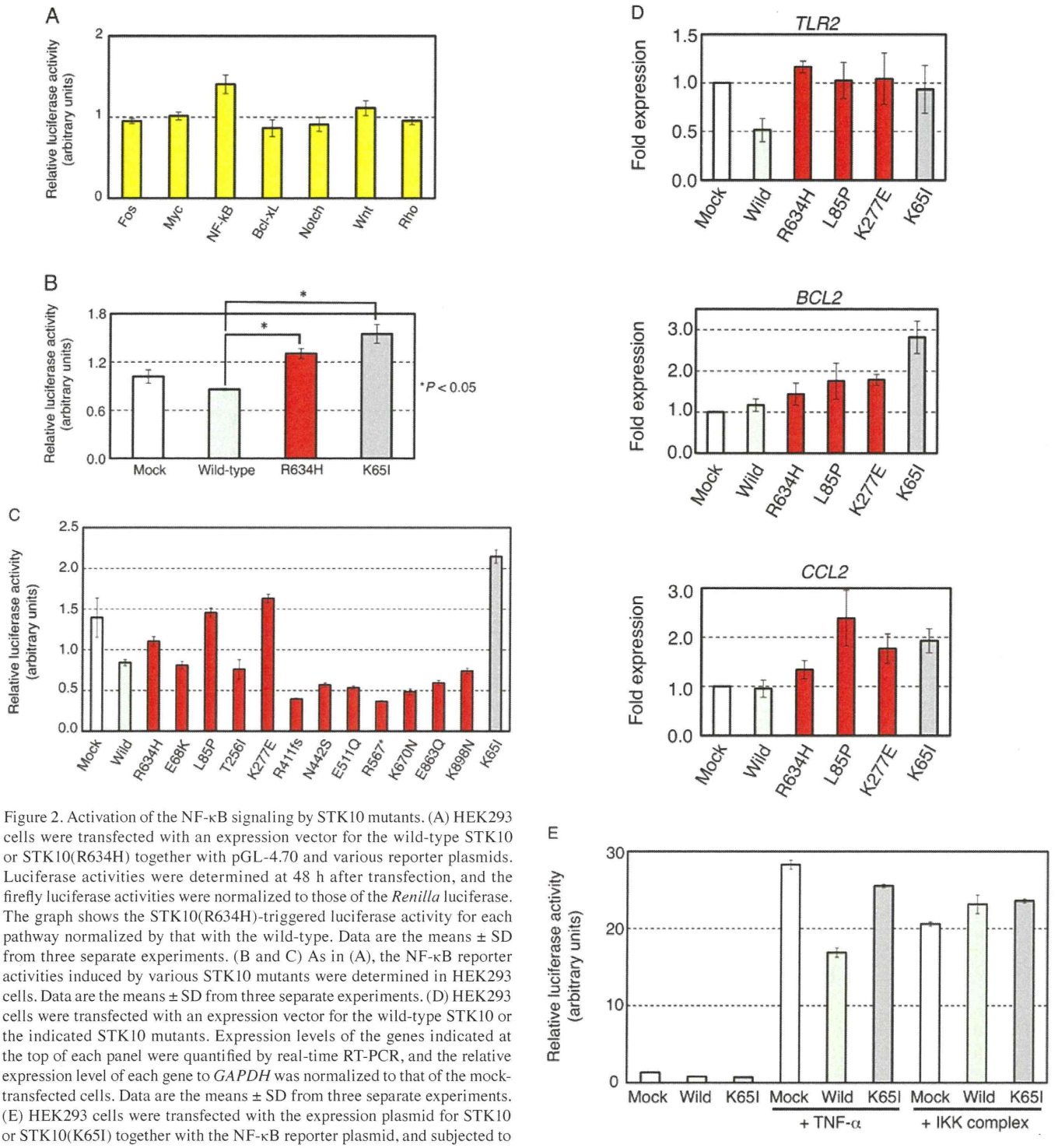

Figure 2. Activation of the NF-κB signaling by STK10 mutants. (A) HEK293 cells were transfected with an expression vector for the wild-type STK10 or STK10(R634H) together with pGL-4.70 and various reporter plasmids. Luciferase activities were determined at 48 h after transfection, and the firefly luciferase activities were normalized to those of the *Renilla* luciferase. The graph shows the STK10(R634H)-triggered luciferase activity for each pathway normalized by that with the wild-type. Data are the means ± SD from three separate experiments. (B and C) As in (A), the NF-κB reporter activities induced by various STK10 mutants were determined in HEK293 cells. Data are the means ± SD from three separate experiments. (D) HEK293 cells were transfected with an expression vector for the wild-type STK10 or the indicated STK10 mutants. Expression levels of the genes indicated at the top of each panel were quantified by real-time RT-PCR, and the relative expression level of each gene to *GAPDH* was normalized to that of the mock-transfected cells. Data are the means ± SD from three separate experiments. (E) HEK293 cells were transfected with the expression plasmid for STK10 or STK10(K651) together with the NF-κB reporter plasmid, and subjected to luciferase assays at 48 h after transfection. Cells transfected with an empty vector (Mock) were similarly analyzed. The same set of cells were either stimulated with 1 ng/ml of TNF-α for 6 h before harvest (the middle panel), or co-transfected with expression plasmids for IKKα, IKKβ and IKKγ (+ IKK complex). Data are the means ± SD from three separate experiments.

(n=56) and the COSMIC database for cancer genome mutations (Release v58, http://cancer.sanger.ac.uk/cancergenome/projects/cosmic/), revealing additional 11 nonsynonymous mutations; E68K in a CML cell line K562, L85P, T256I, R411-frameshift (R411fs), K670N and K898N in various specimens of ovarian cancer, K277E in a testicular cancer specimen, N442S in a pancreatic cancer cell line Pa21C, E511Q in a specimen of upper aerodigestive tract cancer, R567* in Jurkat, and E863Q in a lung cancer specimen (Fig. 1B).

Activation of NF-κB signaling by STK10 mutants. To examine whether STK10(R634H) affects intracellular signaling pathway related to Fos, Myc, NF-κB, Bcl-xL, Notch, Wnt or Rho, we examined the reporter activity for each pathway under the expression of the wild-type or the R634H mutant of STK10. As shown in Fig. 2A, the R634H mutant significantly elevated the NF-κB reporter activity compared to the wild-type ($P<0.05$, Student's t-test), but did not affect the other signaling systems. To further investigate the role of STK10

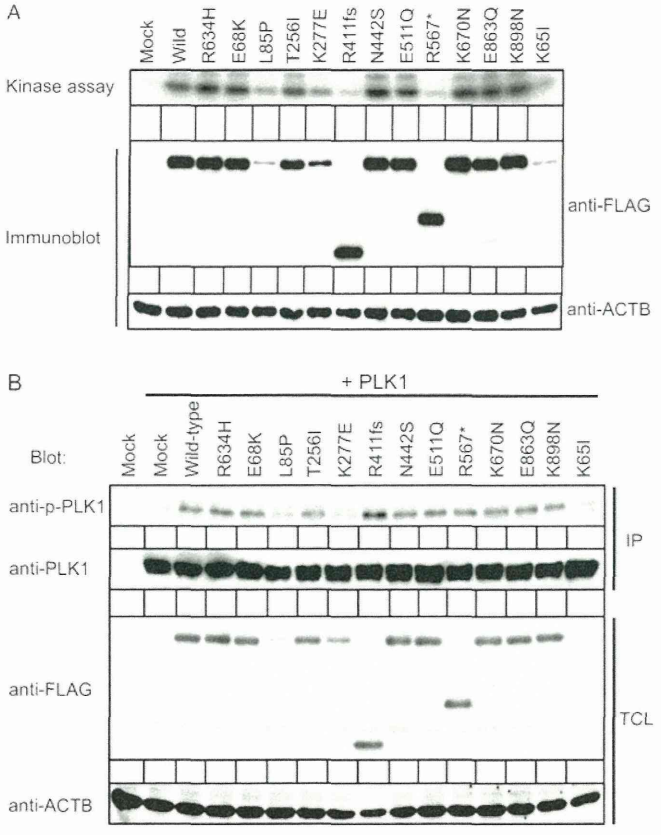

Figure 3. (A) Kinase activities of STK10 mutants. HEK293 cells were transfected with an expression vector for FLAG-tagged wild-type or mutant forms of STK10. Total cell lysates (TCL) were immunoprecipitated with anti-FLAG antibody, and subjected to an *in vitro* kinase assay with histone H2A as a substrate (top panel). TCL of each fraction was separately immunoblotted with antibodies to FLAG or ACTB (lower panel). Cells transfected with an empty vector were similarly analyzed (Mock). (B) HEK293 cells were transfected with an expression plasmid for FLAG-tagged wild-type or mutant forms of STK10 together with that for PLK1 as indicated at the top. TCL was subjected to immunoprecipitation (IP) with antibodies to PLK1, and immunoblotted with the same antibodies (anti-PLK1) or antibodies to the phosphorylated forms of PLK1 (anti-p-PLK1) (top panel). TCLs of the same samples were separately probed with antibodies to either FLAG or ACTB (lower panel).

in the NF-κB signaling, we generated cDNA for a kinase-dead mutant (K65I) of STK10, and examined its effects on the NF-κB signaling. Of note, the wild-type STK10 rather suppressed the NF-κB pathway, but the R634H mutation abolished such effect, suggesting that STK10 is a negative regulator for intracellular NF-κB activity (Fig. 2B). This hypothesis was further reinforced by the fact that the kinase-inactive K65I mutant markedly elevates the NF-κB reporter signaling. We further asked the effects of other STK10 mutants on NF-κB, and revealed that the L85P and K277E mutants found in the COSMIC database clearly induced NF-κB (Fig. 2C). Noteworthy, these mutations were somatically acquired in ovarian and testicular cancers, respectively. The other STK10 mutations did not affect NF-κB signaling (Fig. 2C and data not shown).

To further confirm the effects of STK10 mutants on the NF-κB activation, expression levels of its target genes were quantified among cells expressing the wild-type or mutant forms of STK10 (Fig. 2D). Consistent with the results of luciferase assay, L85P, K277E, R634H and K65I mutants each induced the expression of NF-κB target genes including *TLR2, BCL2* and *CCL2*, compared to the wild-form. These results indicate that polymorphism as well as somatic mutations of STK10 may regulate NF-κB signaling in various human cancers.

It is not clear yet how STK10 regulates the NF-κB pathway. When HEK293 cells were stimulated with tumor necrosis factor (TNF)-α, K65I amino acid change cancelled the STK10-mediated NF-κB suppression (Fig. 2E). However, such regulation was not observed on the IKK complex-driven NF-κB activation, indicating that STK10 may interact with the NF-κB pathway between TNF receptors and the IKK complex.

Kinase activities of STK10 mutants. To examine if the STK10 mutations directly affect its enzymatic activity, FLAG-tagged wild-type or mutant forms of STK10 was expressed in HEK293 cells, and subjected to immunoprecipitation with antibodies to FLAG, followed by an *in vitro* kinase assay with histone H2A as an exogenous substrate. As shown in Fig. 3A, while the wild-type STK10 clearly phosphorylates histone H2A, the L85P, K277E and K65I mutants remarkably attenuate the substrate phosphorylation. We could not, however, observe a notable difference between the wild-type and the R634H mutant in their ability of H2A phosphorylation, suggesting that R634H mutation may regulate the NF-κB signaling not through suppressing its enzymatic activity but through affecting its interaction to other proteins.

Of note, the R411fs and R567* mutants did not phosphorylate histone H2A, indicating the coiled-coil domain and/or carboxyl terminal end of STK10 (Fig. 1B) is indispensable for histone phosphorylation. Immunoblot analysis with antibodies to FLAG revealed that protein amounts of the L85P, K277E and K65I mutants were markedly reduced, which may account for the decreased phosphorylation of histone H2A.

Since STK10 is also known to phosphorylate PLK1 (14), we further investigated the phosphorylation level of PLK1 when co-expressed with the wild-type or mutant forms of SKT10 (Fig. 3B). Consistent with the result of the *in vitro* kinase assay, phosphorylation of PLK1 was reduced under the presence of the L85P, K277E or K65I mutant. Again, R634H mutation did not significantly affect the PLK1 phosphorylation. Strikingly, however, both of R411fs and R567* mutants could phosphorylate PLK1 equally to, or greater than, the wild-type. The carboxyl-terminal half of STK10 may, thus, be dispensable for the phosphorylation of PLK1 *in vivo*.

Anti-apoptotic function of STK10 mutants. NF-κB plays pivotal roles in inflammatory and anti-apoptotic responses in cells, and constitutive NF-κB activation has been recognized as a hallmark of several lymphoid malignancies (15). Given the NF-κB-activating potential of STK10 mutants, we then asked whether such mutants also regulate cell apoptosis. Glucocorticoids are known to be a potent apoptosis-inducer in lymphocytes, and have been used in therapeutic regimens for lymphoid malignancies (15). As shown in Fig. 4A, treatment of a mouse T-cell line, CTLL-2, with dexamethasone inhibited cell proliferation, and, importantly, introduction of the wild-type STK10 markedly augmented such effect, again confirming its tumor-suppressive role. In contrast, introduction

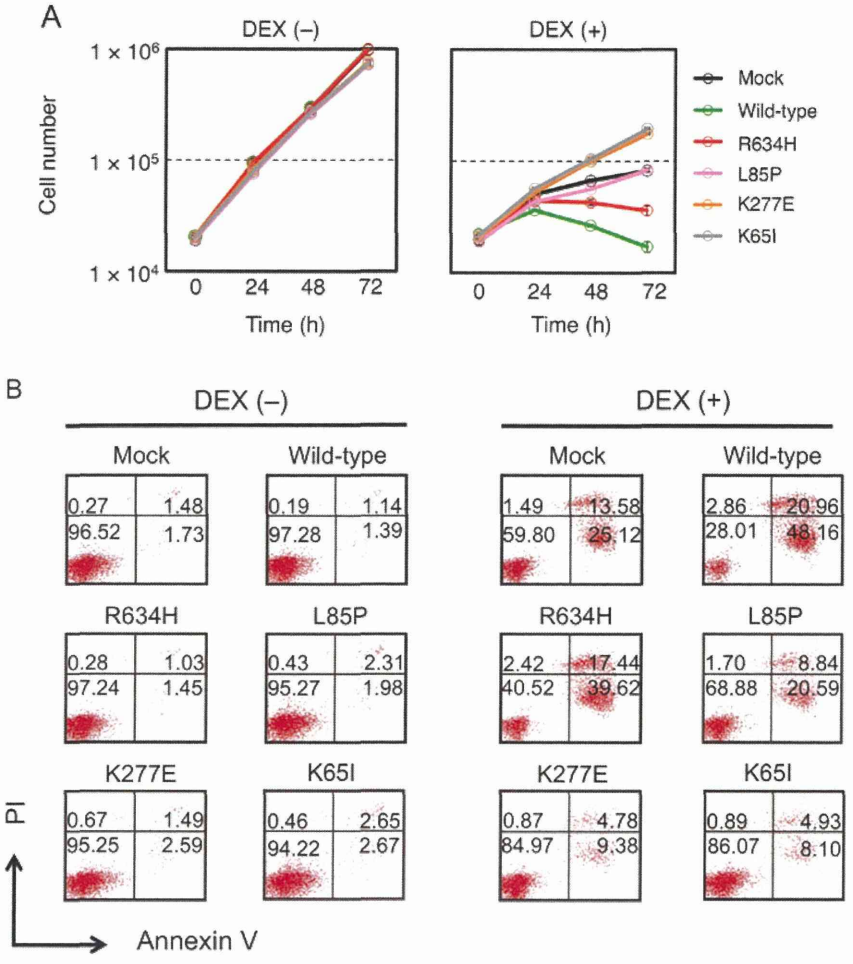

Figure 4. Anti-apoptotic effects of the STK10 mutants. (A) CTLL-2 cells expressing the wild-type STK10 or the indicated STK10 mutants were cultured with 2 ng/ml of IL-2 either in the absence (-) or presence (+) of 1 μM dexamethasone (DEX). The number of viable cells was determined at the indicated times shown at the bottom. Data are means ± SD from three separate experiments. CTLL-2 cells infected with mock retrovirus were similarly analyzed (Mock). (B) CTLL-2 cells at 72 h in (A) were collected and stained with Annexin V/PI, followed by flow cytometry. Positive or negative fractions for Annexin V or PI staining are shown as percentage for each experiment.

of NF-κB-activating mutants restored cell growth, in a parallel manner to their NF-κB-activating potential.

To determine whether the growth-inhibitory effect thus observed was related to apoptosis, we conducted the Annexin V/PI staining assay (Fig. 4B). Although an increase in the Annexin V-positive fraction was apparent in dexamethasone-treated, wild-type STK10-expressing CTLL-2 cells, introduction of the L85P, K277E, R634H or K65 mutant of STK10 significantly suppressed apoptosis. Thus, a part of polymorphism/somatic mutations within STK10 not only activate the NF-κB pathway, but directly exert anti-apoptotic function.

Multiplex deep sequencing of STK10 in PTCL specimens. As it was demonstrated that some STK10 mutations induce NF-κB activation and render resistance to dexamethasone-induced apoptosis, we further searched for *STK10* mutations in genomic DNAs of 92 PTCL specimens. It should be noted, however, that PTCL specimens frequently contain numerous normal cells in addition to neoplastic cells, which makes it difficult to determine the presence or absence of *STK10* mutations with conventional Sanger sequencing. We therefore chose a deep sequencing approach with the GAIIx system (16), leading to the isolation of one specimen carrying STK10(R634H) (data not shown).

Discussion

STK10 is a member of the STE20 family of serine/threonine kinases that are involved in a variety of intracellular functions such as cell proliferation, regulation of apoptosis, rearrangement of the cytoskeleton and cell motility (17). While the Lok kinase, a mouse homolog of STK10, was shown to be highly expressed in lymphocytes (18), expression of STK10 may be detected in other tissues as well, including brain, colon, thymus, kidney, liver, small intestine and lung (14).

In this study, we identified STK10(R634H) in a PTCL specimen, and demonstrated that the R634H mutation induces NF-κB activation. We also demonstrated, for the first time, that the wild-type STK10 is a negative regulator for NF-κB, and may be a tumor suppressor since it strongly augments dexamethasone-driven apoptosis in T-lymphocytes. Given the fact that STK10(R634H) attenuates cell apoptosis, such polymorphism may predispose lymphomagenesis. Indeed, through a mutation search of additional PTCL specimens (n=92), we